Progress In Electromagnetics Research B, Vol. 32, 21–38, 2011

PERFORMANCE OF THE ADAPTIVE NORMALIZED MATCHED FILTER DETECTOR IN COMPOUND-GAUSSIAN CLUTTER WITH INVERSE GAMMA TEXTURE MODEL

A. Younsi* **and M. Nadour**

Ecole Militaire Polytechnique, B. P. 17 Bordj El Bahri, Algiers, Algeria

Abstract—In the present paper, we deal with the performance analysis of the Adaptive Normalized Matched Filter (ANMF) detector in compound-Gaussian clutter with inverse gamma texture model and unknown covariance matrix. First, the maximum likelihood estimate (MLE) of the covariance matrix for this clutter model is derived. The MLE is then plugged into the ANMF test and compared to the well known normalized sample covariance matrix estimate (NSCM) and the approximate maximum likelihood estimate (AML). The performance in terms of CFAR behavior and detection probability is evaluated in the presence of simulated clutter and real sea clutter data, which is collected by the McMaster IPIX radar.

1. INTRODUCTION

In the area of adaptive radar detection, estimating the clutter covariance matrix is a very important task since the detection performance depends directly on the accuracy of this estimate. Adaptive radar detection against Gaussian clutter using the Sample Covariance Matrix estimate(SCM) has been extensively studied in the past [1, 2]. While the SCM is the maximum likelihood estimate of the covariance matrix for Gaussian clutter, its use in the non-Gaussian case leads to a drastic degradation of the detection performance [3]. New advances in radar technology show that the clutter is a non-Gaussian process. For example, the sea clutter observed with high resolution radars (mall range cell size) and/or low grazing angle (less than 10°) exhibits a non-Gaussian behavior [4]. The resolution depends on the radar parameters such as the pulse width and the beam width.

Received 19 May 2011, Accepted 27 June 2011, Scheduled 6 July 2011

* Corresponding author: Arezki Younsi (ayounsi@spg.tu-darmstadt.de).

Results from experimental statistical analysis conducted in [5], showed that sea clutter amplitudes fit a K-distribution for all combinations of frequencies (among X-, S- and L-bands), polarisation (V and H) and waveform resolutions (15 m and 150 m). In [5], investigations of statistical fluctuations of the sea clutter have revealed that for small illuminated patches ($\simeq 100\,\mathrm{m}^2$) and grazing angles ($\simeq 1^\circ$) the distribution of the clutter deviates from the Gaussian law. Similar results were obtained with an other analysis of X-band sea clutter having a range resolution of 33 m and an average grazing angle of 1.56° see [6]. Furthermore, several data sets with different resolutions, grazing angles and frequency bands were analyzed in [7] and well fitted by Weibull distribution.

Radar systems operating in a maritime environment are seriously affected by the presence of sea clutter that interferes with and often completely obscures radar echoes from targets of interest. In addition to its non-Gaussian behavior, the sea clutter exhibits a spiky nature [5], these spikes appear target-like and without some prior knowledge regarding the distribution of the clutter, the performance of standard detection algorithms, such as Constant False Alarm Rate (CFAR), can be seriously degraded [8].

Recently, the compound-Gaussian clutter model was proposed for modeling sea clutter and was successfully tested on several real data sets [9–12]. This model can be interpreted as a product of a real positive random process, named texture, times a complex Gaussian process, usually named speckle. The texture represents the local clutter power whose fluctuations are induced by the spatial and temporal variations in the radar backscattering. The overall probability density function (pdf) of the clutter process depends on that of the texture component. For example the well known K-distribution is obtained when the texture follows a gamma pdf.

Considering this successful model, several estimators of the covariance matrix from secondary data have been proposed in the literature. Conte et al. [13], proposed the Normalized Sample Covariance Matrix estimate (NSCM), which is independent on the texture pdf but depends on the covariance matrix structure. The ML estimator of a K-distributed clutter covariance matrix has already been derived in [14], where Gini et al. have also proposed the Approximate Maximum Likelihood (AML) estimate which is independent on both the texture and the structure of the covariance matrix. This AML estimator was also called the fixed point estimate (FP) in [15].

In this work, we model the clutter as a compound-Gaussian process with inverse gamma texture pdf [16–18] and derive the corresponding ML estimator of the covariance matrix. To compare

this estimator to NSCM and AML, we use it in the ANMF test and analyze its performance in terms of false alarm (P_{fa}) and detection (P_d) probabilities as well as computational complexity. The study is conducted with simulated data as well as with real sea clutter data collected by the McMaster IPIX radar.

2. SIGNAL AND CLUTTER MODELS

The radar detection problem can be seen as a binary hypotheses test

$$\begin{cases} H_0 : \mathbf{z} = \mathbf{d} \\ H_1 : \mathbf{z} = \mathbf{d} + \mathbf{s} \end{cases} \tag{1}$$

where $\mathbf{z} = [z(0), z(1), \ldots, z(N-1)]^T$ is the complex valued vector of N pulses collected by the radar during the time on target, $\mathbf{d}$ is the clutter vector and $\mathbf{s}$ is the signal vector.

We model the useful signal as $\mathbf{s} = \alpha\mathbf{p}$, where α is the complex amplitude of the target return accounting for both channel and target effects. The N dimensional vector $\mathbf{p} = e^{j\boldsymbol{\varphi}}$ is commonly referred to as the time steering vector and the components of the vector $\boldsymbol{\varphi}$ are given by

$$\varphi[k] = 2\pi f_d k T_R, \quad k = 0, \ldots, N-1 \tag{2}$$

where f_d is the target Doppler frequency and T_R the radar pulse repetition time. The classical Swerling-I model of target fluctuation is obtained when α is modeled as a complex Gaussian random vector with zero mean and variance $E[\alpha^2] = \sigma_\alpha^2$.

According to the compound-Gaussian model, the clutter $\mathbf{d}$ is modeled as a product of two independent random variables:

$$\mathbf{d} = \sqrt{\tau}\mathbf{x} \tag{3}$$

where $\mathbf{x}$ is an N dimensional zero-mean complex Gaussian vector representing the speckle component and τ, the texture, is the variance of the underlying conditional Gaussian vector, represents the local clutter power. To each value of τ we associate the pdf $f_\tau(\tau)$, which ultimately determines the non-Gaussian behavior of the clutter. In shorthand notation, we write $\mathbf{x} \sim CN(\mathbf{0}, \mathbf{M})$ where $\mathbf{M} = E[\mathbf{x}\mathbf{x}^H]$ is the normalized (i.e., $[\mathbf{M}]_{ii} = 1$ for $i = 1, \ldots, N$) covariance matrix of the speckle and $(.)^H$ indicates the conjugate transpose operator.

Depending on the texture pdf, several distributions have been used to model real clutter data. The Weibull and the K-distribution are widely used to model sea clutter under the assumption of high resolution radar and/or low grazing angle. In some cases, these two distributions do not fit correctly the real data. This holds in particular

in the tail of the distribution which is of great importance in the design of constant false alarm (CFAR) detectors. Here after we recall the pdfs of the amplitude of these two models and that of the inverse gamma texture model which we will use in this work since it fits well the real data in our possession.

2.1. Gaussian Model

The Gaussian clutter is obtained when $f_\tau(\tau) = \delta(1 - \sigma_G^2)$, where $\delta(\cdot)$ is the Dirac delta function, and σ_G^2 is the variance of the clutter. In other words, in Gaussian clutter, the texture τ, which represents the local power, is no longer random but instead is given by $\tau = \sigma_G^2$ with probability one. Thus $\mathbf{d} \sim CN(\mathbf{0}, \sigma_G^2\mathbf{M})$.

2.2. K-distributed Model

The K-distribution [19] is obtained when the texture is modeled as a Gamma-distributed random variable with mean μ and order parameter ν [10], i.e.,

$$f_\tau(\tau) = \frac{1}{\Gamma(\nu)} \left(\frac{\nu}{\mu}\right)^\nu \tau^{\nu-1} \exp\left(-\frac{\nu}{\mu}\tau\right) u(\tau) \tag{4}$$

where $\Gamma(\cdot)$ is the Gamma function [20]. The parameter μ is called the scale parameter and represents the average clutter power, while ν is called the shape parameter.

The amplitude R follows the K-distribution given by [21]

$$f_R(r) = \frac{\sqrt{2\nu/\mu}}{2^{\nu-1}\Gamma(\nu)} \left(\sqrt{\frac{2\nu}{\mu}} r\right)^\nu K_{\nu-1}\left(\sqrt{\frac{2\nu}{\mu}} r\right) u(r) \tag{5}$$

where $K_\alpha(\cdot)$ is the modified second-kind Bessel function of order α [20].

The moments are given by

$$E\{R^n\} = \left(\frac{2\mu}{\nu}\right)^{n/2} \frac{\Gamma(\nu + n/2)\Gamma(1 + n/2)}{\Gamma(\nu)} \tag{6}$$

2.3. Weibull Model

In this model:

$$f_R(r) = \frac{c}{b}\left(\frac{r}{b}\right)^{c-1} \exp(-(r/b)^c) u(r) \tag{7}$$

$$E\{R^n\} = b^n \Gamma\left(\frac{n}{c} + 1\right) \tag{8}$$

where c is the shape parameter and b is the scale parameter.

There is no closed form for the texture pdf.

2.4. Inverse Gamma Texture Model

This model is obtained when the quantity $\rho = 1/\tau$ follows a gamma pdf given by

$$f_\rho(\rho) = \frac{\rho^{(\alpha-1)}}{\Gamma(\alpha)\beta^\alpha} e^{-\rho/\beta} \tag{9}$$

where α is the shape parameter and β is the scale parameter. The pdf of τ is then obtained from the formula [22]

$$f_\tau(\tau) = \frac{1}{\tau^2} f_\rho\left(\frac{1}{\tau}\right) \tag{10}$$

which gives

$$f_\tau(\tau) = \frac{\tau^{-(1+\alpha)}}{\Gamma(\alpha)\beta^\alpha} e^{-1/\beta\tau} \tag{11}$$

The pdf of the amplitude R can be obtained from

$$f_R(r) = \int_0^{+\infty} f_{R|\tau}(r|\tau) f_\tau(\tau) d\tau \tag{12}$$

where $f_{R|\tau}(r|\tau)$ is a Rayleigh pdf given by

$$f_{R|\tau}(r|\tau) = \frac{2r}{\tau} e^{-r^2/\tau} \tag{13}$$

Inserting (13) and (11) in (12), we obtain after a suitable change-of-variables

$$f_R(r) = \frac{2\alpha\beta r}{(\beta r^2 + 1)^{\alpha+1}} \tag{14}$$

The moments are given by:

$$E\{R^n\} = \left(\frac{1}{\beta}\right)^{n/2} \frac{\Gamma(1 + n/2)\Gamma(\alpha - n/2)}{\Gamma(\alpha)}, \quad n = 1, 2, \ldots \tag{15}$$

3. STATISTICAL ANALYSIS OF REAL SEA CLUTTER DATA

In this section, we perform a statistical analysis of real sea clutter data collected by McMaster University, Canada, IPIX radar in February 1998. IPIX is an experimental X-band search radar, capable of dual polarized and frequency agile operation. The radar site was located east of "Place Polonaise" at Grimsbay, Ontario, looking at lake Ontario from a height of 20 m. The pulse repetition frequency (PRF) is 1000 Hz, the polarization is Linear (H or V) switchable pulse-to-pulse,

simultaneous dual polarization on receive and a cross-polarization isolation of 30 dB. The antenna beam width is 0.9 degrees, the grazing angle is 0.38 degrees, and there are 60000 pulses per cell. We carry out our analysis on several files. Here we show the results corresponding to the file $19980223\_165836\_ANTSTEP$. The range resolution for this file is 30m and the number of range cells is 34 [23].

To get the statistical properties of the real data, we compare the empirical pdf of the amplitude of the data with the K-distribution, the Weibull and the Compound-Gaussian with inverse gamma texture models.

The parameters of the theoretical pdfs are estimated by the method of moments (MoM), which consists of equating the first and second moments with corresponding theoretical ones given in Section 2. The accuracy of fit is evaluated via the root mean-square error (RMSE) defined in [24] by

$$RMSE = \frac{1}{N_p} \sum_{i=1}^{N_p} |f_R(i) - h(i)|^2 \tag{16}$$

Here $f_R(.)$ is the generic pdf whose parameters are estimated from the real data, $h(.)$ is the real data histogram, and i is the generic point of the amplitude axis at which both histogram and pdf are evaluated. The pdf which gives the smallest RMSE value is considered to be the best fit to the data.

The results of the statistical analysis show that the inverse gamma texture model gives the smallest RMSE for all the range cells and all the polarizations considered (see Table 1). In this table, a signals polarization is designated by a two-letter combination TR, where T is the transmitted polarization (H or V) and R is the received polarization (H or V); thus we speak of four kinds of polarization: HH, HV, VH, and VV.

Figure 1 shows the results relative to the 1st range cell for different polarizations. Clearly, the compound-Gaussian model with inverse gamma texture provides a better fit to the data than the Weibull and

Table 1. The RMSE values.

	HH	VV	VH	HV
K PDF	0.0627	0.0124	0.0224	0.0209
Weibull PDF	0.0359	0.0080	0.0269	0.0239
Inv. gam. tex. PDF	0.0071	0.0039	0.0041	0.0041

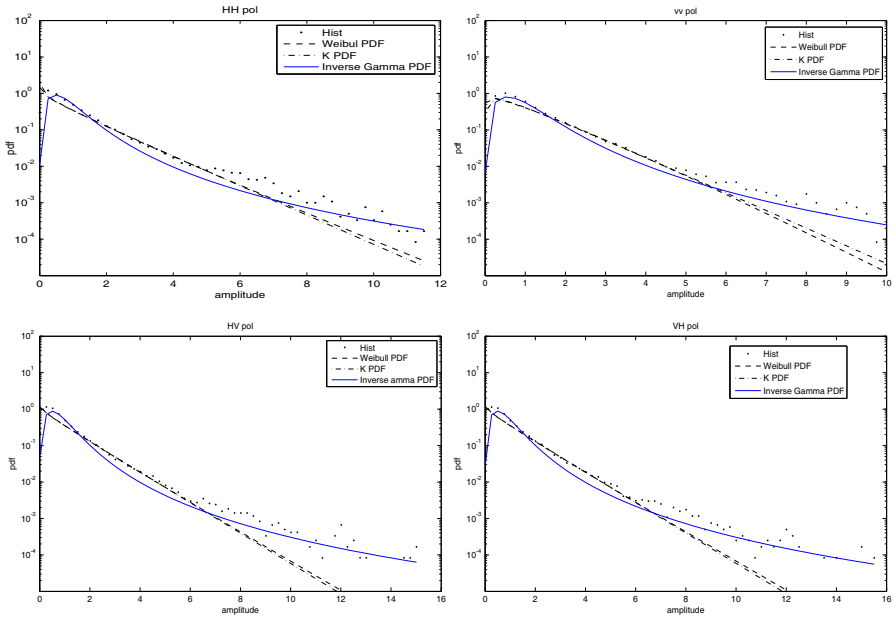

Figure 1. Amplitude pdf analysis, HH, VV, HV and VH polarizations, 1st range cell.

the K-distributions and in particular at the distribution tail. This model was also tested successfully with another real data set having a resolution of 3 m [18].

In addition to the above pdf fitting, we check the validity of the inverse gamma pdf for modeling the texture component. To this end, we estimate the texture from the real data and compare its empirical pdf to both the theoretical inverse gamma and the gamma densities.

The entire sequence of the considered range cell data is divided in N_B bursts of N pulses. The texture value in the kth burst is then estimated according to

$$\hat{\tau}_k = \frac{1}{N} \sum_{i=0}^{N-1} |z_k(i)|^2, \qquad k = 1, \ldots, N_B \tag{17}$$

where $z_k(i) = z((k-1)N + i)$.

Figure 2 shows the empirical texture histogram compared to the inverse gamma and the gamma pdfs. The results show a good fit of the inverse gamma pdf. This reinforces the validity of the assumed clutter model.

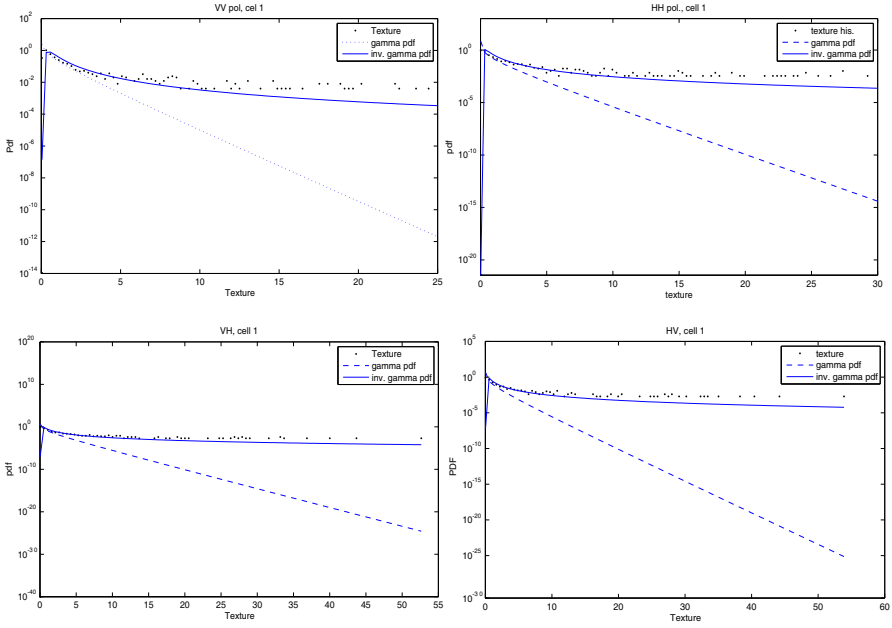

Figure 2. Texture pdf analysis, HH, VV, HV and VH polarizations, 1st range cell.

Previous analysis of real sea clutter data pointed out that horizontally polarized data is spikier than vertically polarized data. Recall that smaller is the shape parameter of a distribution, spikier is the corresponding data. For the processed data, we have, like in [18], estimated the shape parameter α of the inverse-gamma distribution for the four type of polarizations. We found $\alpha = 1.419$ for HH data, $\alpha = 1.645$ for VV data and $\alpha = 1.454$ for both HV and VH data. The spiky nature of the clutter is more evident with HH data and it seems that the cross-polarization data HV and VH have the same properties and are spikier than VV data.

4. THE ADAPTIVE DETECTION ALGORITHM

When the covariance matrix $\mathbf{M}$ of the clutter is assumed *a priori* known, a statistic test, which is widely used for Gaussian as well as compound-Gaussian clutter for the detection problem (1), is the

Normalized Matched Filter (NMF) [13, 25, 26].

$$\Lambda(\mathbf{z}) = \frac{\left|\mathbf{p}^H\mathbf{M}^{-1}\ \mathbf{z}\right|^2}{|\mathbf{p}^H\mathbf{M}^{-1}\mathbf{p}|\,|\mathbf{z}^H\mathbf{M}^{-1}\mathbf{z}|} \underset{H_0}{\overset{H_1}{\gtrless}} \gamma \tag{18}$$

The scale invariance property of this test makes it CFAR to the texture component of the clutter. In practice, the covariance matrix is seldom known, The ANMF is obtained by replacing $\mathbf{M}$ in the NMF by an appropriate estimate $\hat{\mathbf{M}}$ from secondary data. The estimate $\hat{\mathbf{M}}$ should maintain the scale invariance characteristic of the statistic test and at the same time provide a CFAR property to the structure of the covariance matrix. In what follows, we recall the existing estimators for the covariance matrix of a compound-Gaussian clutter and we derive the maximum likelihood estimate for the special case of the inverse gamma texture model.

4.1. Estimation of the Covariance Matrix

In a practical adaptive radar system, the covariance matrix of the clutter is estimated from a set of secondary data, which must be representative of the samples in the cell under test (CUT). The secondary data is often taken from L cells that are just in the neighborhood of the CUT, and due to this geographical proximity, these cells share approximately the same covariance structure.

4.1.1. Maximum Likelihood Estimation of the Covariance Matrix

Let $\mathbf{z}_i = \sqrt{\tau_i}\mathbf{x}_i$; $i = 1, \ldots, L$ be the L samples from secondary cells to be used to estimate the unknown covariance matrix. Starting from the joint pdf of these L i.i.d training data vectors, it was shown in [14] that the ML estimate of the covariance matrix is solution to the equation

$$\hat{\mathbf{M}}_{ML} = \frac{1}{L}\sum_{i=1}^{L} c_N\left(\mathbf{z}_i^H\hat{\mathbf{M}}_{\mathbf{ML}}^{-1}\mathbf{z}_i\right)\cdot\mathbf{z}_i\mathbf{z}_i^H \tag{19}$$

with

$$c_N(x) = h_{N+1}(x)/h_N(x) \tag{20}$$

and

$$h_N(x) = \int_0^{+\infty} \tau^{-N}\exp(-x/\tau)f_\tau(\tau)d\tau \tag{21}$$

To find this solution, Gini et al. [14] proposed an iterative algorithm given by

$$\hat{\mathbf{M}}_{ML}[k+1] = \frac{1}{L}\sum_{i=1}^{L} c_N\left(\mathbf{z}_i^H\hat{\mathbf{M}}_{\mathbf{ML}}^{-1}[k]\mathbf{z}_i\right)\cdot\mathbf{z}_i\mathbf{z}_i^H \tag{22}$$

where k is the k^{th} iteration. In the same paper, the authors developed a closed form expression for the coefficient $c_N(x)$ for the special case of a K-distributed clutter. In the present paper, we derive a closed form expression for this coefficient for a clutter with inverse gamma texture pdf.

We substitute in (21) the expression of $f_\tau(\tau)$ from (11) to get

$$h_N(x) = \int_0^{+\infty} \tau^{-N} \exp(-x/\tau) \frac{\tau^{-(1+\alpha)}}{\Gamma(\alpha)\beta^\alpha} \exp(-1/\beta\tau) d\tau \tag{23}$$

By setting $a = x + \frac{1}{\beta}$ and $b = N + \alpha$, we get

$$h_N(x) = \frac{1}{\Gamma(\alpha)\beta^\alpha} \int_0^{+\infty} \frac{1}{\tau^{b+1}} \exp(-a/\tau) d\tau \tag{24}$$

Using the change of variable $q = a/\tau$, we obtain

$$\begin{aligned} h_N(x) &= \frac{1}{\Gamma(\alpha)\beta^\alpha a^b} \int_0^{+\infty} q^{b-1} e^{-q} dq \\ &= \frac{\Gamma(b)}{\Gamma(\alpha)\beta^\alpha a^b} \\ &= \frac{\Gamma(N+\alpha)}{\Gamma(\alpha)\beta^\alpha (x+\frac{1}{\beta})^{N+\alpha}} \end{aligned} \tag{25}$$

From (20) we have

$$c_N(x) = \frac{\Gamma(N+\alpha+1)}{\Gamma(N+\alpha)(x+1/\beta)} \tag{26}$$

and using the identity $\Gamma(N+\alpha+1) = (N+\alpha)\Gamma(N+\alpha)$, we obtain the closed form

$$c_N(x) = \frac{N+\alpha}{x+\frac{1}{\beta}} \tag{27}$$

4.1.2. The Approximate Maximum Likelihood Estimation of the Covariance Matrix

The AML estimate of the covariance matrix [14] is obtained by replacing the weighting coefficients $c_N(\mathbf{z}_i^H \hat{\mathbf{M}}_{\mathbf{ML}}^{-1} \mathbf{z}_i)$ in (22) by the coefficient $\frac{N}{\mathbf{z}_i^H \hat{\mathbf{M}}_{AML}^{-1} \mathbf{z}_i}$ to get

$$\hat{\mathbf{M}}_{AML}(k+1) = \frac{N}{L} \sum_{i=1}^{L} \frac{\mathbf{z}_i \mathbf{z}_i^H}{\mathbf{z}_i^H \hat{\mathbf{M}}_{\mathbf{AML}}^{-1}(k) \mathbf{z}_i} \tag{28}$$

4.1.3. Normalized Sample Covariance Matrix

The NSCM was proposed in [13] and is given by

$$\hat{\mathbf{M}}_{NSCM} = \frac{N}{L} \sum_{i=1}^{L} \frac{\mathbf{z}_i \mathbf{z}_i^H}{\mathbf{z}_i^H \mathbf{z}_i} \tag{29}$$

While the NSCM is independent only of the texture component of the clutter [3], the AML is independent of both the texture and the covariance matrix structure [14, 15].

5. PERFORMANCE ANALYSIS AND CFAR PROPERTIES

In this section, we evaluate the detection performance of the ANMF with the ML, AML and NSCM estimators of covariance matrix. In the first step, the analysis is conducted with simulated data according to the compound-Gaussian model with inverse gamma texture pdf. In the second step, we consider the real sea clutter data analyzed in Section 3.

5.1. Performance with Simulated Data

We simulate a compound-Gaussian clutter with inverse gamma texture pdf where the covariance matrix of the speckle component (covariance structure of the clutter) is given by

$$[\mathbf{M}]_{i,j} = \rho^{|i-j|} \tag{30}$$

where ρ is the one lag correlation coefficient.

Figures 3 and 4 display the ANMF P_{fa} versus threshold plot for several values of ρ. We observe that the performance of the ANMF with both AML and ML estimates of the covariance matrix does not depend on ρ, while NSCM performance does. Fig. 5 depicts P_{fa} against normalized Doppler frequency ($f_d T_R$) of the time steering vector. The three estimators maintain a nearly constant false alarm. The AML and ML estimators exhibit a very similar performance while NSCM exhibit a peak near zero frequency. This peak can be explained by the fact that the NSCM, as it was stated before, is sensitive to the covariance matrix structure (30), in other terms to the correlation coefficient ρ. One can notice that the power spectral density (PSD) of the simulated clutter is located around zero frequency (it is an AR process of order one) and if we set a threshold (for a specified P_{fa}) out of the PSD band width, the P_{fa} will increase if the Doppler frequency of the time steering vector approaches the center of this band. The AML and ML estimators are independent on the covariance matrix structure so they

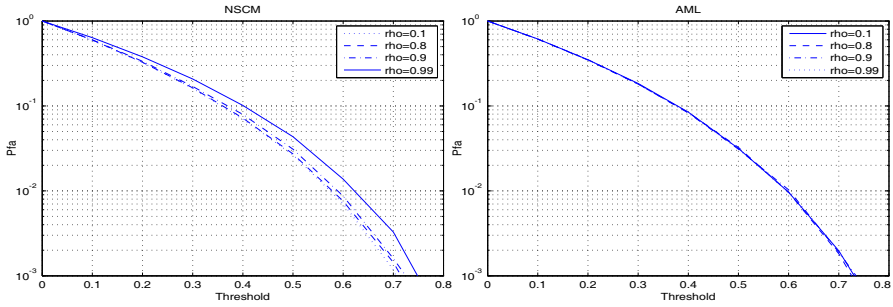

Figure 3. P_{fa} against threshold with NSCM and AML estimators for different values of ρ. $N = 8$, $L = 24$, $f_d T_R = 0.5$, $\alpha = 1.7$ and $\beta = 1$.

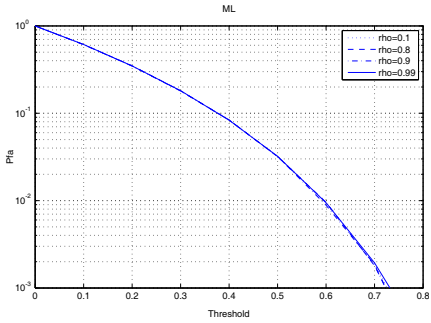

Figure 4. P_{fa} against threshold with ML estimator for different values of ρ. $N = 8$, $L = 24$, $f_d T_R = 0.5$, $\alpha = 1.7$ and $\beta = 1$.

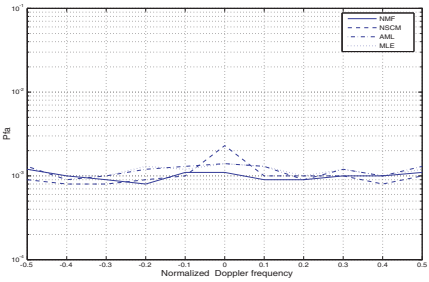

Figure 5. P_{fa} against normalized Doppler frequency. $N = 8$, $L = 24$, $\alpha = 1.7$, $\beta = 1$ $\rho = 0.9$ and $P_{fa} = 10^{-3}$.

exhibit a constant P_{fa}. Other values of N, L and f_d have been used leading to the same comparison (results not shown here for lack of space). Fig. 5 also displays the clairvoyant NMF plot, which assumes $\mathbf{M}$ is known.

5.2. Performance with Real Data

We now consider the detection performance of the ANMF in the presence of real sea clutter data. The procedure used to estimate P_{fa} and P_d is shown in Fig. 6. Each data file is composed of N_t temporal returns from N_c range cells and stored in an $N_t \times N_c$ complex matrix. We consider an $N \times (L + 1)$ data window, where N is the number of pulses and L the number of secondary cells used to estimate the

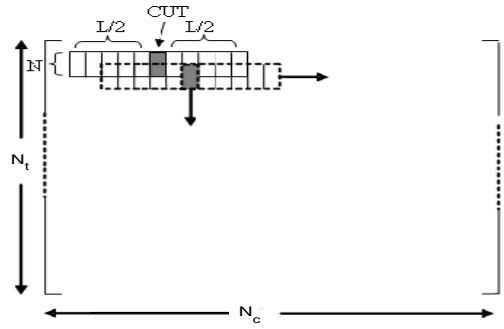

Figure 6. The experimental procedure used to evaluate P_{fa} and P_d.

covariance matrix. The CUT is set in the middle of the window. The data window is slid in space from range bin to range bin and in time with an overlap of $N/2$ samples until the end of the data set. To evaluate the actual false alarm probability, we perform the ANMF test for each data window, with the CUT containing only clutter. The actual P_{fa} is then given by the ratio of the total number of times the test exceeds the threshold and the total number of trials. Moreover, for evaluating the the detector performances we assume $N = 8$, $L = 16$ (the case $L = 24$ or greater has not been considered due to the lack of a sufficient number of trials for obtaining reliable estimates of $\hat{P}_{fa}$) and set the threshold for a nominal false alarm of $P_{fa} = 10^{-3}$. The parameters α and β in (27) are estimated from real data using the MoM (see [18]). The number of iterations K in the iterative algorithm (22) and (28) is taken to be equal to 3 see [14] and [18].

Figure 7 displays $\hat{P}_{fa}$ against normalized Doppler frequency for the four data set polarimetric channels. We observe a mismatch between $\hat{P}_{fa}$ and the nominal P_{fa}, which is heavier when f_d belongs to the frequency range where the clutter PSD is significantly different from the noise floor (see Fig. 8). The curves corresponding to the AMl and Ml estimates almost coincide.

The main cause for the P_{fa} degradation is the spatial and temporal non-stationarity of the sea clutter [24, 27]. Owing to this phenomenon, the secondary range bins used in the estimation of the covariance matrix do not share the same spectral properties. Hence, the estimated matrix departs from the true matrix [27]. Other possible sources of degradation can be attributed to the fact that the model is not perfectly compound-Gaussian and may be the texture and the speckle are not independent.

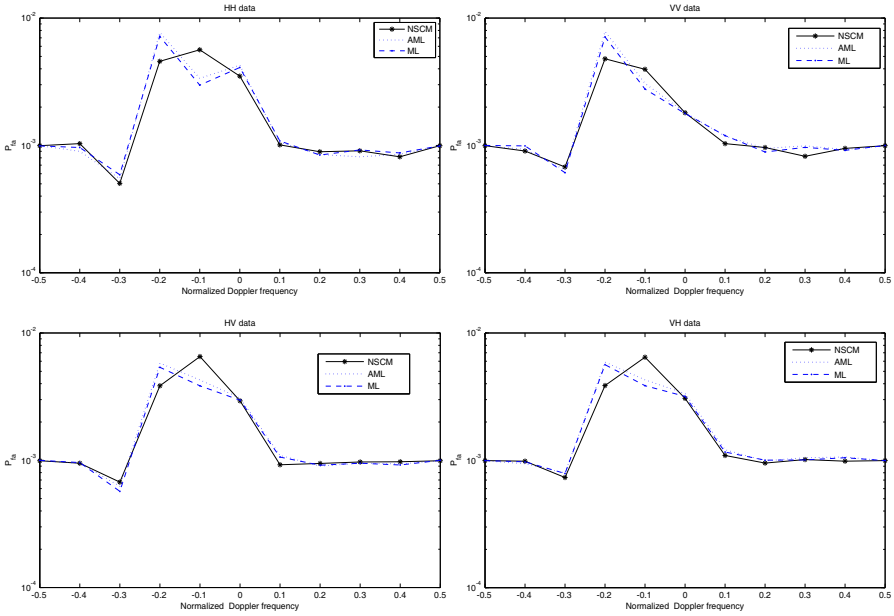

Figure 7. P_{fa} against normalized Doppler frequency. HH, VV, HV and VH data, with $N = 8$, $L = 16$ and nominal $P_{fa} = 10^{-3}$.

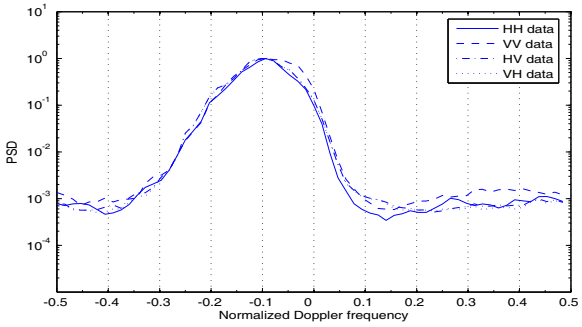

Figure 8. PSD of the 1st cell.

Now, we evaluate the probability of detection by injecting a synthetic target in the CUT such that its content can be written as $\mathbf{z} = \mathbf{s} + \mathbf{d}$. We use the Swerling I model $\mathbf{s} = \alpha\mathbf{p}$ where α and $\mathbf{p}$ were defined in Section 2. We choose the Doppler frequency f_d of the target such that the normalized Doppler frequency $f_d T_R = 0.5$ ($T_R = 1/PRF$). Fig. 9 shows P_d against signal to clutter ratio

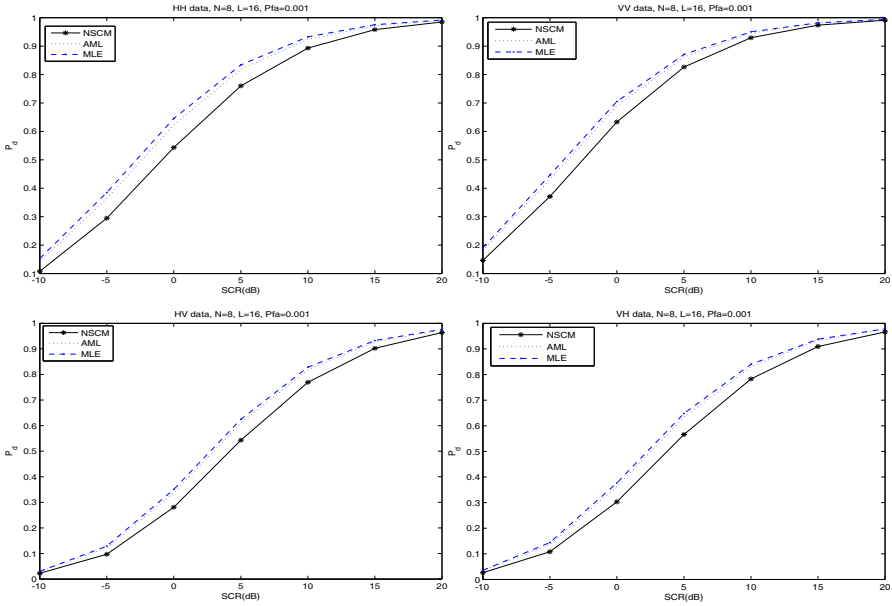

Figure 9. P_d against SCR, HH, VV, HV and VH data, $f_d T_R = 0.5$, $N = 8$, $L = 16$, $P_{fa} = 10^{-3}$.

(SCR)for the four polarimetric channels. Here also the AML and ML estimates exhibit approximately the same performance outperforming the NSCM.

Regarding the implementation, the ML estimator involves more computational complexity than AML and NSCM estimators.

6. CONCLUSIONS

In the present paper, we have analyzed the performance of the ANMF detector with different covariance matrix estimators in non-Gaussian clutter modeled as a compound-Gaussian process with inverse gamma texture model. This model was tested successfully on real data sets with different polarizations. In addition to the existing NSCM and AML estimators of the covariance matrix, we have derived the maximum likelihood estimate of the covariance matrix for the special case of inverse gamma texture model. In the case of simulated clutter, the results showed that the three estimators maintain approximately the CFAR property of the detector. The AML and the ML estimators exhibit the same performance and they do not depend on the value of the correlation coefficient ρ of the clutter while the NSCM does. In

the presence of real data, the CFAR property is no longer maintained for the three estimators. This mismatch was attributed to the spatial and temporal non-stationarity of the clutter. Finally, among the three estimators, the AML estimate represents a good tradeoff between performance and computational complexity.

ACKNOWLEDGMENT

The authors would like to express their sincere thanks to Dr. C. DEBES (Darmstadt University of Technology, Germany) and Dr. N. HANOUN (USTHB Algeria) for their helpful comments and to Prof. M. GRECO (Pisa University, Italy) who kindly provided the real data.

REFERENCES

1. Kelly, E. J., "An adaptive detection algorithm," *IEEE Transactions on Aerospace and Electronic Systems*, Vol. 23, 115–127, Nov. 1986.
2. Kraut, S., L. L. Scharf, and T. Mcwhorter, "Adaptive subspace detetcors," *IEEE Transactions on signal Processing*, Vol. 49, No. 1, 1–16, 2001.
3. Gini, F., "Performance analysis of two structured covariance matrix estimators in compound-Gaussian clutter," *Signal Processing*, Vol. 80, 365–371, 2000.
4. Chan, H. C., "Radar sea-clutter at low grazing angles," *IEE Proceedings*, Vol. 137, Pt. F, No. 2, 102–112, April 1990.
5. Watts, S., "special issue on radar clutter and multipath propagation," *IEE Proc. part F*, Vol. 138, No. 2, 1991.
6. Stehwien, W., "Statistics and correlation properties of high resolution X-band sea clutter," *IEEE Radar Conference*, 1994.
7. Sekine, M. and Y. Mao, *Weibull Radar Clutter*, IEE Radar, Sonar, Navigation Avionics, Series 3, 1990.
8. Skolnik, M. I., *Introduction to Radar Systems*, 2nd edition, McGraw-Hill, New York, NY, 1980.
9. Nohara, T. J. and S. Haykin, "Canadian East Coast radar trials and the K-distribution," *IEE Procedings*, Part F, Vol. 138, No. 2, 80–88, 1991,
10. Farina, A., F. Gini, M. Greco, and L. Verrazzani, "High resolution sea clutter data: A statistical analysis of recorded live data," *IEE Proc. Radar Sonar Navigation*, Vol. 144, No. 3, 121–130, 1997.
11. Conte, E., A. Demaio, and C. Galdi, "Statistical analysis of

real clutter at different range resolutions," *IEEE Transactions on Aerospace and Electronic Systems*, Vol. 40, No. 3, 903–918, 2002.

12. Greco, M., F. Gini, and M. Rangaswamy, "Statistical analysis of measured polarimetric clutter data at different range resolutions," *IEE Proc. Radar Sonar Navigation*, Vol. 153, No. 6, 473–481, 2006.
13. Conte, E., M. Lops, and G. Ricci, "Asymptotically optimum radar detection in compound-Gaussian clutter," *IEEE Transactions on Aerospace and Electronic Systems*, Vol. 31, No. 2, 617–625, 1995.
14. Gini, F. and M. Greco, "covariance matrix estimation for CFAR detection in heavy tailed clutter," *Signal Processing*, Vol. 82, 1495–1507, 2002.
15. Pascal, F., Y. Chitour, J. P. Ovarlez, P. Forster, and P. Larbazal, "Covariance structure maximum likelihood estimates in compound-Gaussian noise: Existance and algorithm analysis," *IEEE trans. signal processing*, Vol. 56, No. 1, 34–48, 2008.
16. Wang, J., A. Dogandzic, and A. Nehorai, "Maximum likelihood estimation of compound-Gaussian clutter and target parameters," *IEEE Transactions on Signal Processing*, Vol. 54, No. 10, October 2006.
17. Balleri, A. and A. Nehorai, "Maximum likelihood estimation for compound-Gaussian clutter with inverse gamma texture," *IEEE Trans. AES*, Vol. 43, No. 2, 775–780, 2007.
18. Younsi, A., M. Greco, F. Gini, and A. Zoubir, "Performance analysis of the adaptive matched subspace detector: An experimental analysis," *IET Radar Sonar and Navigation*, Vol. 3, No. 3, 195–202, 2009.
19. Jakeman, E. and P. N. Pusey, "A model for non-Rayleigh sea echo," *IEEE Transactions on Antennas and Propagation*, Vol. 24, 806–814, 1976.
20. Abramovitz, M. and I. A. Stegun, *Handbook of Mathematical Functions with Formulas, Graphs, and Mathematical Tables*, Dover Publications, New York, 1965.
21. Gradshteyn, I. S. and I. M. Ryzhik, *Table of Integrals, Series, and Products*, 5th edition, Academic Press, New York, 1994.
22. Papoulis, A., *Random Variable and Stochastic Processes*, McGraw-Hill, New York, 1984.
23. http://soma.crl.mcmaster.ca/ipix/.
24. Greco, M., F. Bordoni, and F. Gini, "X-band sea-clutter nonstationarity: Influence of long waves," *IEEE Journal of Oceanic Engineering*, Vol. 29, No. 2, 269–283, 2004.
25. Sangston, K. J., F. Gini, M. V. Greco, and A. Farina,

"Structures for radar detection in compound Gaussian clutter," *IEEE Transactions on Aerospace and Electronic Systems*, Vol. 35, 445–458, 1999.

26. Gini, F., "Sub-optimum coherent radar detection in a mixture of K-distributed and Gaussian clutter," *IEE Procedings*, Part F, Vol. 144, No. 1, 39–48, 1997.
27. Greco, M., F. Gini, A. Younsi, M. Rangaswamy, and A. Zoubir, "Non-stationary sea clutter: Impact on disturbance matrix estimate and detector CFAR," *IEEE Proc. Int. Conf. Radar*, Adelaide, Australia, 2008